Obrabotka metallov (tekhnologiya, oborudovanie, instrumenty) = Metal Working and Material Science. 2025 vol. 27 no. 4 pp. 180–193
ISSN: 1994-6309 (print) / 2541-819X (online)
DOI: 10.17212/1994-6309-2025-27.4-180-193

NSTU NETI

Obrabotka metallov - Metal Working and Material Science

Journal homepage: http://journals.nstu.ru/obrabotka_metallov

Investigation of the effect of process parameters on photochemical machining of SS316l for manufacturing vascular stents

Devendra Agrawal [1, a, *], ***Sushil Patil*** [1, b], ***Dinesh Washimkar*** [2, c], ***Nitin Ambhore*** [2, d], ***Dhroov Agrawal*** [3, e]

[1] Department of Mechanical Engineering, S.V.P.M'S College of Engineering Malegaon (Bk.), Savitribai Phule Pune University, Pune, Maharashtra, 413115, India
[2] Department of Mechanical Engineering, Vishwakarma Institute of Technology, Savitribai Phule Pune University, Pune, Maharashtra, 411037, India
[3] Department of Bachelor of Medicine & Bachelor of Surgery, KD Medical College Mathura, Uttar Pradesh, 281406, India

[a] https://orcid.org/0000-0002-2477-1841, dpagrawal@engg.svpm.org.in; [b] https://orcid.org/0000-0002-0547-6038, sspatil@engg.svpm.org.in;
[c] https://orcid.org/0000-0002-1312-2619, dinesh.washimkar@vit.edu; [d] https://orcid.org/0000-0001-8468-8057, nitin.ambhore@vit.edu;
[e] https://orcid.org/0009-0000-8547-9484, dhroovagrawal109@gmail.com

ARTICLE INFO

Article history:
Received: 26 October 2025
Revised: 28 October 2025
Accepted: 15 November 2025
Available online: 15 December 2025

Keywords:
PCM
Phototool
Taguchi
Etching
Stent
Vein blockage

ABSTRACT

Introduction. Photochemical machining (*PCM*) is a non-traditional machining method capable of developing burr-free and stress-free biomedical components. A stent is a small meshed tube used to remove blockages and open blood passages in arteries and veins. *SS316L* is one of the recommended materials for stents due to its biocompatibility and machinability with photochemical processes. Vascular stents are made from metal mesh, fabric, silicone, or combinations of materials. **The purpose of this work** is to investigate the effect of process parameters on the *PCM* process during the machining of *SS316L* and to manufacture an *SS316L* stent as a substrate using photochemical machining. The manufactured stent is used in larger arteries, such as the aorta, to provide a stable channel for blood flow. **Methods of investigation.** The process parameters for the photochemical machining process were optimized using the *Taguchi* method with an L_9 experimental array (*DoE*). The effect of process parameters on responses was investigated using ***F***-values. An *ANN* was employed as a predictive tool for observing deviations in the responses. **Results and discussion.** The optimum set of machining parameters was obtained and utilized for manufacturing the vascular stent. A phototool with the required stent strut size was developed using CAD software. Controlled etching with ferric chloride generated the mesh, and laser seam welding was performed to develop the tubular stent for placement in blockages. The dimensions of the developed stent were measured with *SEM*, and the stent strut size was found to vary from 312 μm to 900 μm.

For citation: Agrawal D., Patil S., Washimkar D., Ambhore N., Agrawal D. Investigation of the effect of process parameters on photochemical machining of SS316l for manufacturing vascular stents. *Obrabotka metallov (tekhnologiya, oborudovanie, instrumenty) = Metal Working and Material Science*, 2025, vol. 27, no. 4, pp. 180–193. DOI: 10.17212/1994-6309-2025-27.4-180-193. (In Russian).

Introduction

One of the significant risks to human health is vascular disease. Cerebrovascular stents are primarily of two types: self-expanding and balloon-expandable. However, both have been associated with issues such as stent migration, vascular injury, and complications related to sudden expansion and contraction within the vessel. While balloon-expandable stents offer precise placement, ease of use, and high radial force, their flexibility in navigating tortuous arteries is limited. There is a clinical need to establish a permanent blood flow pathway in branch vessels through the placement of a permanent vascular stent. The stent implantation procedure involves deploying a mesh-like device into the diseased or occluded segment of the blood vessel. Once positioned at the target lesion, the stent restores and maintains patency by providing mechanical support to the narrowed or blocked lumen, ensuring sustained blood flow.

*** Corresponding author**
Agrawal Devendra Prabhudayal, Ph.D. (Engineering), Associate Professor
S.V.P.M'S College of Engineering Malegaon (Bk.),
Savitribai Phule Pune University, Pune,
Maharashtra, 413115, India.
Tel.: +91-9421054282, **e-mail**: dpagrawal@engg.evpm.org.in

Because human vasculature varies significantly among individuals, a standard stent often does not conform precisely to a patient's specific vascular anatomy. The conventional tubular mesh may require customized sizing. Although self-expanding stents offer flexibility and good wall apposition, their complex deployment procedure can lead to prolonged operation times and an increased risk of embolic stroke. Vascular stents can be fabricated from metals, polymers, or composites and typically feature uniform unit-cell designs, sizes, and shapes. *Alizera* et al. designed and developed three innovative hybrid auxetic stents and analyzed their behavior under quasi-static loading. The stents were fabricated using the fused deposition modeling (*FDM*) additive manufacturing technique. A comparison between experimental and finite element simulation results showed good agreement [1].

Canic et al. developed a novel mathematical and computational framework for geometrically optimized mesh-like stents. These stents are modeled as a network of one-dimensional curved rods, approximated by piecewise straight rods to simplify computation [2]. *Ebrahimi* et al. explored the tailoring of metamaterial stents for biomedical applications. These findings hold considerable potential for advancing stent technology, ultimately benefiting patients with conditions such as arterial stenosis [3]. *Pang* et al. established a micro-milling process route for magnesium alloy cardiovascular stents and evaluated the machined stents' mechanical properties and quality [4].

Li et al. investigated the fabrication of vascular stents using various *AM* techniques and materials, including cost-effective bio-inert metals, bioresorbable polymers, and bioresorbable metals. The study highlighted the potential of *AM* to produce patient-specific stents with unique unit-cell designs, leading to improved conformability and crimping-expansion performance [5]. *Yan* et al. developed stents for curved arteries and performed multi-objective optimization of process parameters to enhance overall stent performance [6].

Roxanne et al. investigated the influence of *FDM* process parameters – such as line width, print speed, and travel speed – on stent quality. By controlling these parameters, stents could be produced in close compliance with the original *CAD* designs. The study concluded that *FDM's* ability to process medical-grade materials offers promising prospects for 3D-printed stents [7]. *Demir* et al. provided an overview of metallic stent manufacturing using laser-based processes, including additive laser powder bed fusion and subtractive laser cutting. The authors emphasized the potential for enhanced collaboration between engineers and clinicians in the biomedical implant industry [8].

Antonio et al. studied the effect of the dip-coating process on the properties of *PCL*/*PLA* composite tubes for stent fabrication. Dynamic mechanical analysis and degradation studies revealed the limitations of pure *PCL* and *PLA*, while the composite tube exhibited behavior more aligned with stent requirements [9].

Despite these advances, the aforementioned methods present certain constraints, including high cost, multi-stage processing, residual stress formation, specialized environment and operator skill requirements, material limitations, and the need for post-processing. To address these challenges, photochemical machining (*PCM*) – a non-traditional microfabrication technique–has been employed for the development of vascular stents. *PCM* has emerged as an efficient alternative to conventional machining for producing thin components with complex geometries [10]. The process involves selective etching of a substrate using a photoresist and etchant [11]. *Fadaei* et al. reported improved surface quality and material removal rate during *PCM* of stainless steel 304 using triethanolamine (*TEA*) as an etchant [12]. *Allen* et al. established performance criteria and metrics for industrial etchants [13]. *Cakir* investigated the parametric effects of etching aluminum with ferric chloride ($FeCl_3$) etchant [14]. *Agrawal* et al. optimized *PCM* parameters for machining *SS304* with $FeCl_3$ etchant, identifying ideal conditions for fabricating microfluidic channels and micromolds with features down to 100 μm [15].

The literature indicates that *PCM* offers several advantages: it is burr-free and stress-free, eliminating the need for post-machining treatment. It is a unique method for machining thin, complex profiles at low cost. The process can be controlled by optimizing parameters, and it leaves the metallurgical properties of the material unaffected. To explore *PCM's* capabilities, the authors have applied it to vascular stent fabrication.

In the present study, the authors attempt to manufacture a vascular stent using the photochemical machining process. All steps – including centrifugal photoresist coating, drying, controlled etching, and *UV* exposure – were conducted in the laboratory. A phototool with stent strut dimensions was designed using *CAD* software and printed using a high-*DPI* precision printer. Ferric chloride etchant was used with parameters optimized via *Taguchi* analysis to produce a mesh with specified dimensions. An artificial neural network (*ANN*) model was developed to predict output parameters, and prediction errors were estimated. Laser seam welding was employed to join the mesh edges into a tubular structure. Stent dimensions were measured using scanning electron microscopy (*SEM*), revealing strut sizes ranging from 312 μm to 900 μm. The manufactured stent is intended for use in larger arteries, such as the aorta, to provide a stable conduit for blood flow.

Methods

SS316L is a widely recommended material for biomedical implants due to its excellent corrosion resistance, biocompatibility, favorable mechanical properties, and broad applicability. It is also well-suited for the photochemical machining (*PCM*) process. The chemical composition of *SS316L* includes: *Mo* (2–3 %), *Si* (≤0.75 %), *N* (0.10%), *P* (≤0.045 %), *C* (≤0.03%), *Ni* (10–14%), *Cr* (16–18 %), with the balance being *Fe*. The *PCM* process involves several steps: material selection, phototool and specimen preparation, photoresist coating (masking), drying, controlled etching, stripping, and inspection, all conducted in a darkroom and laboratory environment. For this study, *SS316L* sheets with dimensions of 30 mm × 30 mm and a thickness of 0.08 mm were used. The phototool consisted of a black circular pattern with a diameter of 10 mm. The artwork was designed using *CAD* software and printed with a high-*DPI* printer. The key process parameters for evaluation were etching time (min), etchant temperature (°C), and etchant concentration (g/L) [16].

Preliminary experiments were conducted using a **one-factor-at-a-time approach** to determine appropriate parameter levels for the design of experiments (*DoE*), with three replicates for each condition [17]. The resulting parameter levels are shown in Table 1. Measurements from the *DoE* are presented in Table 2.

Table 1

Process parameters and their levels

Parameters	Level 1	Level 2	Level 3
Concentration (g/L)	300	400	500
Time (min)	2	3	4
Temperature (°C)	50	55	60

Table 2

Experimental design matrix

Sr. No.	Conc. (g/L)	Time (min)	Temp. (°C)	*MRR* (mm^2/min)	Undercut (mm)	Depth of cut (mm)	Etch Factor
1	300	2	50	2.88	0.018	0.0366	2.0333
2	300	3	55	3.12	0.058	0.0396	0.6843
3	300	4	60	3.88	0.098	0.0493	0.5037
4	400	2	55	4.91	0.031	0.0623	2.0045
5	400	3	60	5.12	0.033	0.0651	1.9860
6	400	4	50	5.28	0.039	0.0671	1.7223
7	500	2	60	5.15	0.033	0.0655	2.0037
8	500	3	50	5.78	0.035	0.0732	2.0857
9	500	4	55	6.12	0.038	0.0823	2.1466

Undercut (Uc)

Undercut is an undesirable machining artifact in *PCM*, resulting from isotropic etching beneath the photoresist mask. As illustrated in Fig. 1, while etching is intended for area ***A***, the process extends laterally under the mask, effectively machining area ***B***. This excess removal is termed undercut (*Uc*) and is quantified using Equation. U_c was measured using a video measuring machine (*VMM*) (Fig. 2). The *VMM* image (Fig. 3) clearly shows two concentric circles: the inner circle corresponds to the phototool dimensions, while the outer circle represents the undesired material removal due to undercut.

$$\boldsymbol{Uc} = 1/2(\boldsymbol{B}-\boldsymbol{A})$$

PCM for stent manufacturing

An optimal set of parameters – namely, an etchant temperature of 50 °C, a concentration of 500 g/L, and an etching time of 2 minutes – was used to achieve the best results. To maintain a uniform etchant concentration throughout the tank, compressed air was bubbled through the solution from the bottom.

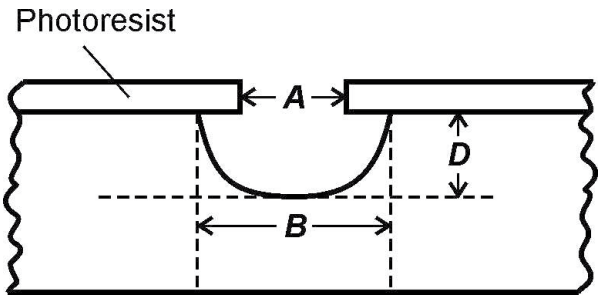

Fig. 1. Definition of undercut (*Uc*), where: ***A*** is the area for machining; ***B*** is the actual machined area

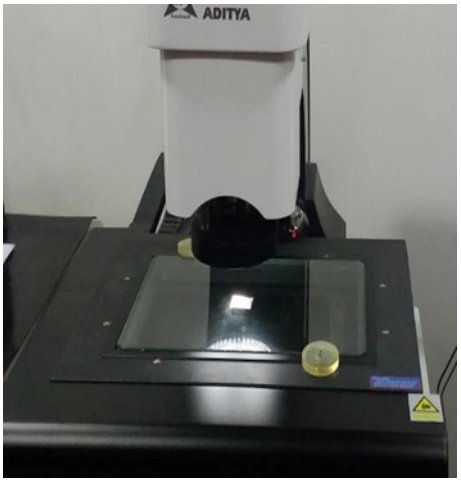

Fig. 2. Specimen under *VMM*

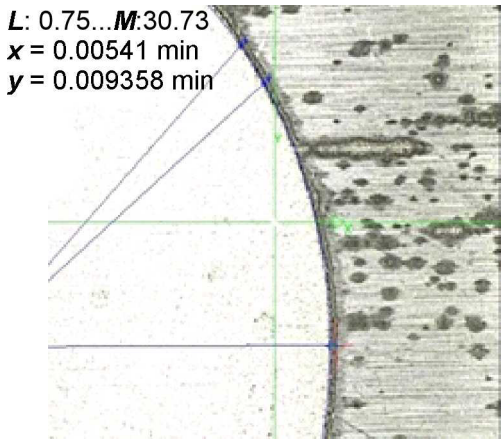

Fig. 3. Specimen showing the inner circle (phototool size) and the outer circle (extra machining)

During etching, the specimen was held in a polymer mesh bag. All necessary safety precautions were observed during the drying, *UV* exposure, and controlled etching stages. Gentle rinsing was employed to remove the etchant and the exposed photoresist. A mesh pattern (stent strut) matching the dimensions specified in the phototool was etched onto the specimen. Any remaining photoresist was removed via soft cleaning with water. A view of the phototool used for stent fabrication is shown in Fig. 4.

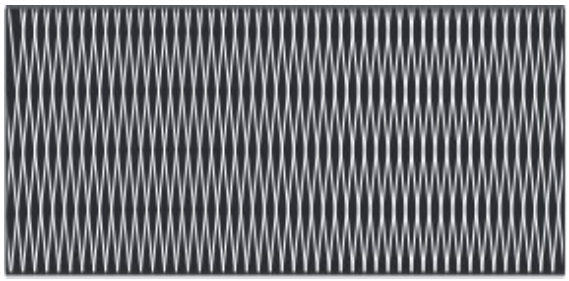

Fig. 4. Phototool used for stent manufacturing

To form a tubular structure, the flat, etched mesh specimen was wrapped around a cylindrical mandrel with a diameter corresponding to the desired stent diameter (ranging from 100 μm to 1,000 μm). The edges of the mesh were aligned and overlapped. A continuous, micro-seam weld was then created along the joint line using laser welding technology. This laser-welded tube ensures a seamless joint. Upon expansion, the stent provides a stable conduit, allowing blood to flow through the stent lumen and its struts within the vessel.

Results and Discussion

The parameter effects and *ANOVA* analysis for undercut are shown in Tables 3 and 4. The *ANOVA* results indicate that etching time is the most significant parameter affecting undercut, followed by etchant concentration. The rate of interaction between the solute (active species in the etchant) and the solvent (substrate) increases with time. The dissolution of material along grain boundaries in the heterogeneous substrate is more pronounced over longer durations. Material removal proceeds more rapidly in the lateral direction (beneath the photoresist mask) than in the vertical direction. Consequently, undercut increases with etching time.

Table 3

Undercut parameters and their levels

Parameters	Level 1	Level 2	Level 3
Concentration (g/L)	0.0580	0.0343	0.0353
Temp. (°C)	0.0306	0.0424	0.0545
Time (min)	0.0272	0.0419	0.0584

Table 4

***ANOVA* table for undercut**

Factor	*D.F.*	*S.S.*	*M.S.*	*F*	*P*
Concentration (g/L)	2	0.00107	0.00053	1.14	0.467
Temp. (°C)	2	0.00145	0.00072	1.54	0.394
Time (min)	2	0.00084	0.00042	0.90	0.526
Error	2	0.00094	0.00047		
Total	8	0.00432			

The parameter effects and *ANOVA* analysis for *MRR* are presented in Tables 5 and 6. It is observed that etchant concentration is the most significant process parameter for *MRR*, followed by etching time [18]. The density of active ferric ions increases with higher etchant concentration. A greater quantity of these ions accelerates the reaction rate. As the frequency of collisions between active ions and the metallic substrate rises, the diffusion of active atoms is enhanced. This directly influences the *MRR* as a key response characteristic. Therefore, as the concentration gradient of the etchant increases, the *MRR* exhibits an upward trend.

Table 5

***MRR* parameters and their levels**

Parameters	Level 1	Level 2	Level 3
Concentration (g/L)	2.368	4.712	4.716
Temp. (°C)	4.310	4.673	5.093
Time (min)	3.293	5.102	5.681

Table 6

ANOVA* table for *MRR

Factor	*D.F.*	*S.S.*	*M.S.*	*F*	*P*
Concentration (g/L)	2	9.3246	4.6623	53.53	0.018
Temp. (°C)	2	0.9144	0.4572	5.25	0.160
Time (min)	2	0.0098	0.0049	0.06	0.947
Error	2	0.1742	0.0871		
Total	8	10.423			

The parameter effects and *ANOVA* analysis for the etch factor are shown in Tables 7 and 8. Etchant concentration is identified as the most significant parameter for the etch factor. The etch factor is defined as the ratio of depth of cut to undercut. Since the increase in depth of cut with rising concentration is more pronounced than the corresponding increase in undercut, the etch factor shows an increasing trend with higher etchant concentration. Based on the *ANOVA* analysis, the optimum machining parameters for *SS316L* using ferric chloride etchant are determined as: etching time of 2 minutes, etchant temperature of 50 °C, and etchant concentration of 500 g/L.

Table 7

Etch factor parameters and their levels

Parameters	Level 1	Level 2	Level 3
Concentration (g/L)	1.0737	1.9042	2.0786
Temp. (°C)	1.9471	1.6117	1.4977
Time (min)	2.0138	1.5853	1.4574

Table 8

***ANOVA* table for etch factor**

Factor	*D.F.*	*S.S.*	*M.S.*	*F*	*P*
Concentration (g/L)	2	1.7300	0.8650	2.79	0.264
Temp. (°C)	2	0.5094	0.2547	0.82	0.549
Time (min)	2	0.3273	0.1636	0.53	0.655
Error	2	0.6208	0.4908		
Total	8	3.1875			

Regression and artificial neural network (*ANN*) models were developed to predict process performance. The percentage error between experimental and predicted values was found to be satisfactory for all response parameters (as shown in Fig. 5) [19]. The error between experimental and predicted results was less than 15 % (as illustrated in Figs. 6, 7, and 8). The maximum error values were 1.781, 0.001, and 0.170, and the minimum error values were 0 for *MRR*, undercut (*Uc*), and etch factor, respectively (as detailed in Tables 9, 10, and 11).

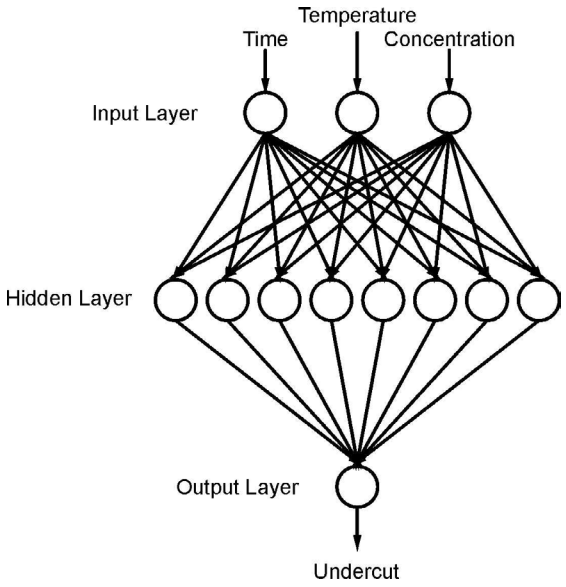

Fig. 5. *ANN* Architecture for undercut

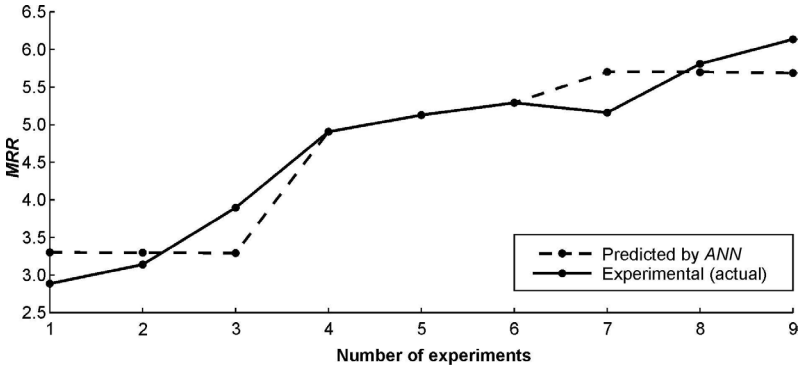

Fig. 6. Implementation of the *ANN* model for prediction of *MRR* (mm³/min)

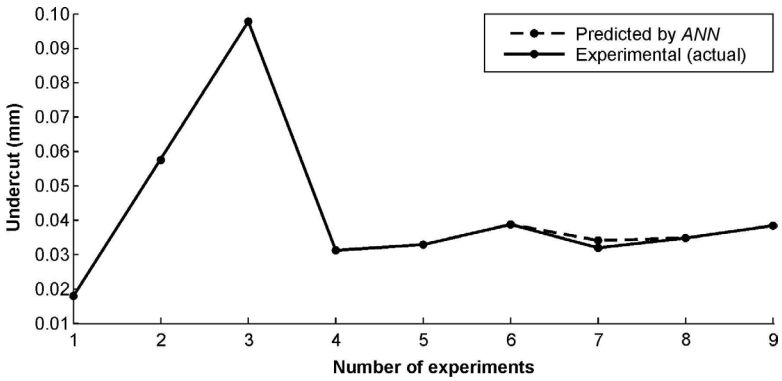

Fig. 7. Implementation of the *ANN* model for prediction of undercut (***Uc***) (mm)

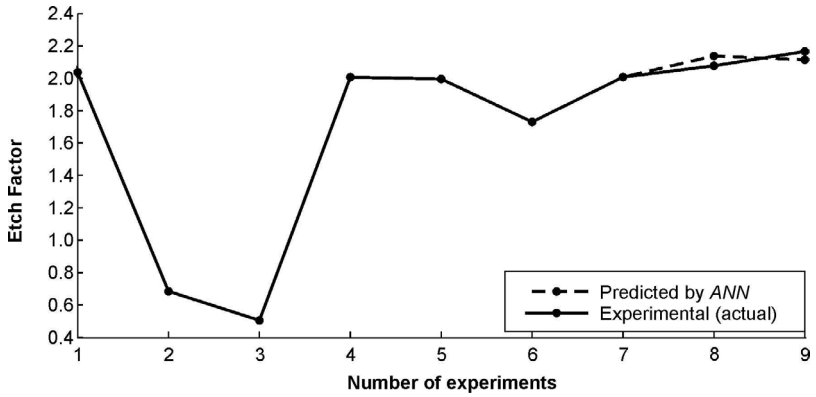

Fig. 8. Implementation of the *ANN* model for prediction of Etch Factor (*EF*)

Table 9

Comparison of actual and predicted *MRR* values and calculated errors

Actual (*MRR*)	2.88	3.12	3.88	4.91	5.12	5.28	5.15	5.78	6.12
Predicted (*MRR*)	3.29	3.29	3.29	4.91	5.12	5.28	5.68	5.68	5.68
Error	1.25	0.52	1.781	0	0	0	0.93	0.17	0.76

Table 10

Comparison of actual and predicted undercut (*Uc*) values and calculated errors

Actual (***Uc***)	0.01	0.05	0.09	0.03	0.03	0.03	0.03	0.03	0.03
Predicted (***Uc***)	0.01	0.05	0.09	0.03	0.03	0.03	0.031	0.03	0.03
Error	0	0	0	0	0	0	0.001	0.001	0

Table 11

Comparison of actual and predicted etch factor (*EF*) values and calculated errors

Actual (*EF*)	2.033	0.684	0.503	2.003	1.986	1.722	2.003	2.098	2.146
Predicted (*EF*)	2.033	0.684	0.503	2.003	1.986	1.722	2.003	2.122	2.146
Error	0	0	0	0	0	0	0	0.170	0

A stent in tubular form was manufactured in the laboratory using photochemical machining**.** Various measurements were performed using scanning electron microscopy (*SEM*)**,** and the stent observations were recorded. A stent strut is a part of the stent designed to open a narrowed or occluded artery. The strut's shape and thickness are crucial for the stent's durability and influence the risk of restenosis. It was observed that the etching process produces a mesh with vertical and horizontal gaps, which is capable of withstanding blood pressure and providing a conduit for blood flow. The undercut generated during etching contributes to weight reduction without compromising the stent's strength. Vessel wall injury is also reduced due to the decreased contact area between the stent and the vein wall. Stent expansion is maintained owing to the work hardening/strain hardening effect induced during the transformation of the flat specimen into a tube. The flat ends provide a suitable surface for laser seam welding.

In Fig. 9, the stent mesh structure – comprising vertical and horizontal struts and the gaps between them – is observed under scanning electron microscopy. Measurements indicate a maximum horizontal strut width of 994.1 μm and a vertical mesh gap of 361.1 μm. The etched specimen shown in Fig. 9 was subsequently formed into a tubular shape.

As shown in Fig. 10, the dimensions of a reference (commercial) stent are measured as 340 μm and 1.1 mm. The dimensions of the *PCM*-manufactured stent closely resemble those of stents produced by conventional methods. Fig. 11 (*SEM* image) reveals that in the tubular (deployed) form, the stent struts align accurately with each other, ensuring unimpeded blood flow through all sections of the stent. The strut width measured across the side edge is 352.8 μm. Due to symmetric double-sided exposure and etching, the mesh pattern is consistent and matches perfectly along the stent's edge. Fig. 12 illustrates the elliptical cross-section of a vertical stent strut, with a major (vertical) axis dimension of 1.137 mm and a minor (horizontal) axis dimension of 318 μm. For comparison, the dimensions of a standard stent strut are provided in Fig. 10.

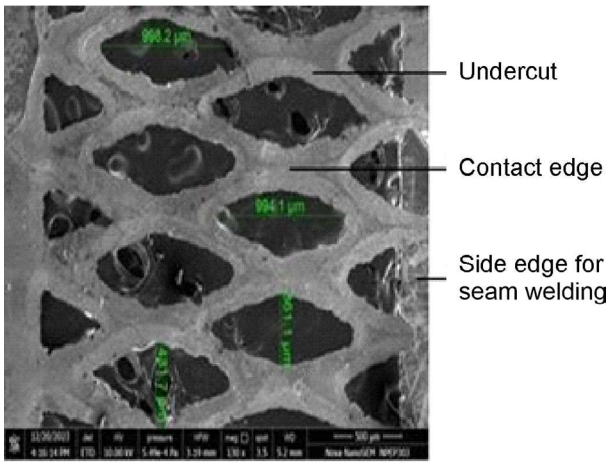

Fig. 9. Observation of vertical and longitudinal stent struts in tubular mesh

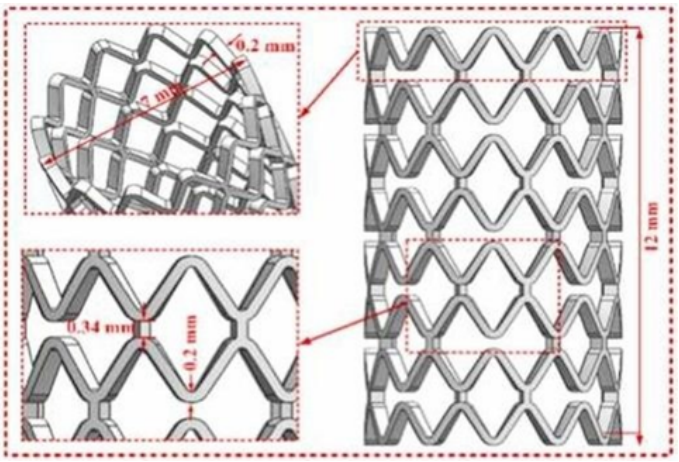

Fig. 10. Standard-sized stent used in vein blockages. (Courtesy of [20])

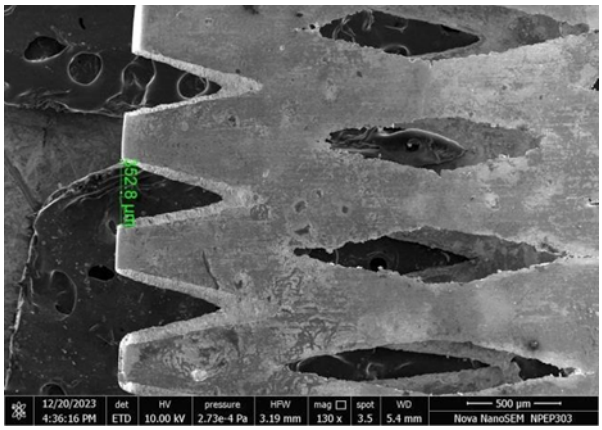

Fig. 11. Observation of longitudinal stent strut

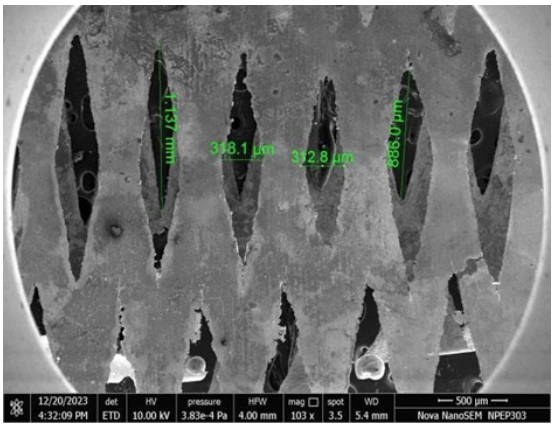

Fig. 12. Observation of vertical stent strut

Conclusion

The key finding of this study is that photochemical machining (*PCM*) can be successfully applied to biomedical applications, such as stent manufacturing. The optimal set of machining parameters for *SS316L* steel was determined to be an etchant temperature of 50 **°C**, an etchant concentration of 500 g/L, and an etching time of 2 minutes. Through precise phototool fabrication**,** *UV* exposure**,** and controlled etching on biocompatible material, a tubular mesh structure (stent struts) was produced, designed to fit within arterial blood vessels to restore or maintain blood flow through blocked veins. The authors achieved a stent strut width of up to 994.1 μm in the vertical direction and a mesh gap of 361.1 μm in the horizontal direction.

For future work, formal medical certification of the stent will be required, adhering to stringent manufacturing and quality control standards. This approach holds significant promise for patients, as the *PCM*

process offers high cost-effectiveness in mass production. Consequently, stent costs could be substantially reduced, improving affordability and accessibility. The application of *PCM* in stent development marks a significant milestone in the advancement of non-traditional machining techniques for medical device fabrication.

References

1. Zamani M.M.A., Etamadi E., Bodaghi M., Hu H. Conceptual design and analysis of novel hybrid auxetic stents with superior expansion. *Mechanics of Materials*, 2023, vol. 187, pp. 1–16. DOI: 10.1016/j.mechmat.2023.104813.

2. Čanić S., Grubišić L., Ljulj M., Maretić M., Tambača J. Geometric optimization of vascular stents modeled as networks of 1D rods. *Journal of Computational Physics*, 2023, vol. 494, pp. 1–32. DOI: 10.1016/j.jcp.2023.112497.

3. Ebrahimi M.S., Noruzi M., Hamzehei R., Etemadi E., Hashemi R. Revolutionary auxetic intravascular medical stents for angioplasty applications. *Materials & Design*, 2023, vol. 235, pp. 1–17. DOI: 10.1016/j.matdes.2023.112393.

4. Pang S., Zhao W., Qiu T., Liu W., Jiao L., Wang X. Study on surface quality and mechanical properties of micro-milling WE43 magnesium alloy cardiovascular stent. *Journal of Manufacturing Processes*, 2023, vol. 101, pp. 1080–1090. DOI: 10.1016/j.jmapro.2023.06.061.

5. Li Y., Shi Y., Lu Y., Li X., Zhou J., Zadpoor A.A., Wang L. Additive manufacturing of vascular stents. *Acta Biomaterialia*, 2023, vol. 167, pp. 16–37. DOI: 10.1016/j.actbio.2023.06.014.

6. Wang Y., Yan C., Mei D., Li Y., Sheng K., Wang J., Wang L., Zhu S., Guan S. Optimized structure design of asymmetrical Mg alloy cerebrovascular stent with high flexibility. *Smart Materials in Manufacturing*, 2024, vol. 2, p. 100040. DOI: 10.1016/j.smmf.2023.100040.

7. Khalaj R., Tabriz A.G., Junqueira L.A., Okereke M.I., Douroumis D. 3D printed stents using fused deposition method. *Journal of Drug Delivery Science and Technology*, 2024, vol. 97, p. 105724. DOI: 10.1016/j.jddst.2024.105724.

8. Demir A.G., Previtali B. Lasers in the manufacturing of cardiovascular metallic stents: Subtractive and additive processes with a digital tool. *Procedia Computer Science*, 2023, vol. 217, pp. 604–613. DOI: 10.1016/j.procs.2022.12.256.

9. Guerra A.J., San J., Ciurana J. Fabrication of PCL/PLA composite tube for stent manufacturing. *Procedia CIRP*, 2017, vol. 65, pp. 231–235. DOI: 10.1016/j.procir.2017.03.339.

10. Chanmanwar R.M., Balasubramaniam R., Wankhade L.N. Application of manufacturing of microfluidic devices: review. *International Journal of Modern Engineering Research*, 2013, vol. 3 (2), pp. 849–856.

11. Çakır O. Etchants for chemical machining of aluminium and its alloys. *Acta Physica Polonica A*, 2019, vol. 135 (4), pp. 586–587. DOI: 10.12693/APhysPolA.135.586.

12. Tehrani F.A., Imanian E. A new etchant for the chemical machining of St304. *Journal of Materials Processing Technology*, 2004, vol. 149 (1–3), pp. 404–408. DOI: 10.1016/j.jmatprotec.2004.02.055.

13. Allen D., Almond H. Characterisation of aqueous ferric chloride etchants used in industrial photochemical machining. *Journal of Materials Processing Technology*, 2004, vol. 149 (1–3), pp. 238–245. DOI: 10.1016/j.jmatprotec.2004.02.044.

14. Cakir O. Chemical etching of aluminum. *Journal of Materials Processing Technology*, 2008, vol. 199 (1–3), pp. 337–340. DOI: 10.1016/j.jmatprotec.2007.08.012.

15. Agrawal D., Kamble D. Optimization of photochemical machining process parameters for manufacturing microfluidic channel. *Materials and Manufacturing Processes*, 2019, vol. 34 (1), pp. 1–7. DOI: 10.1080/10426914.2018.1512115.

16. Wangikar S.S., Patowari P.K., Misra R.D. Effect of process parameters and optimization for photochemical machining of brass and German silver. *Materials and Manufacturing Processes*, 2016, vol. 32 (15), pp. 1747–1755. DOI: 10.1080/10426914.2016.1244848.

17. Jadhav P.K., Sahai R.S.N., Solanke S., Gawande S.H. Multi-objective optimization of EN19 steel milling parameters using Taguchi, ANOVA, and TOPSIS approach. *Journal of Alloys and Metallurgical Systems*, 2024, vol. 7, p. 100102. DOI: 10.1016/j.jalmes.2024.100102.

18. Jatti V.S., Singarajan V., Saiyathibrahim A., Jatti V.S., Krishnan M.R., Jatti S.V. Enhancement of EDM performance for NiTi, NiCu, and BeCu alloys using a multi-criteria approach based on utility function. *Obrabotka metallov (tekhnologiya, oborudovanie, instrumenty) = Metal Working and Material Science*, 2025, vol. 27, no. 2, pp. 57–88. DOI: 10.17212/1994-6309-2025-27.2-57-88. (In Russian).

19. Anita J., Das R., Pradhan M.K. Multi-objective optimization of electrical discharge machining processes using artificial neural network. *Jordan Journal of Mechanical and Industrial Engineering*, 2016, vol. 10 (1), pp. 11–18.

20. Ji H., Zhang W., Li Z., Chai M., Wang Y. Experimental study of NiTi alloy cardiovascular stent formed via SLM. *Materials Today Communications*, 2024, vol. 41, p. 110426. DOI: 10.1016/j.mtcomm.2024.110426.

Conflicts of Interest

The authors declare no conflict of interest.